Published in final edited form as:

Eur J Nucl Med Mol Imaging. 2015 January ; 42(1): 97–102. doi:10.1007/s00259-014-2897-1.

Reduced retention of Pittsburgh compound B in white matter lesions

Lidia Glodzik, MD, PhD[1,2,*], **Henry Rusinek, PhD**[2], **Jinyu Li**[2], **Cyrus Zhou**[1], **Wai Tsui, MS**[1], **Lisa Mosconi, PhD**[1], **Yi Li, MD**[1], **Ricardo Osorio, MD**[1], **Schantel Williams, RN**[1], **Catherine Randall, MA**[1], **Nicole Spector, BA**[1], **Pauline McHugh, MD**[1], **John Murray, BS**[1], **Elizabeth Pirraglia, MA**[1], **Shankar Vallabhajolusa, PhD**[3], and **Mony de Leon, EdD**[1]

[1]Center for Brain Health, Department of Psychiatry, New York University School of Medicine, New York, USA

[2]Department of Radiology, New York University School of Medicine, New York, USA

[3]Department of Radiology, Weill Cornell Medical College, New York, USA

Abstract

Purpose—One of the interesting features of amyloid tracer Pittsburgh compound B (PiB) is that it generates a signal in the white matter (WM) in both healthy subjects and cognitively impaired individuals. This characteristic gave rise to the possibility that PiB can be used to trace WM pathology. In a group of cognitively healthy elderly, we examined PiB retention in normal-appearing WM (NAWM) and white matter lesions (WML), one of the most common brain pathologies in aging.

Methods—We segmented WML and NAWM from fluid attenuation inversion recovery (FLAIR) images of 73 subjects (age 61.9±10.0, 71% women). PET-PiB images were corrected for partial volume effects and coregistered to FLAIR images and WM masks. WML and NAWM PiB signals were then extracted.

Results—PiB retention within WML was lower than in NAWM ($p<.001$, 14.6% reduction). This was true both for periventricular WML ($p<.001$, 17.8% reduction) and deep WML ($p=.001$, 7.5% reduction).

Conclusions—PiB binding in WM is influenced by the presence of WML, which lower the signal. Our findings add to the growing evidence that PiB can depict WM pathology and prompt further investigations into PiB binding targets in WM.

Keywords

Pittsburgh compound B; white matter; white matter lesions; healthy elderly

[*]Corresponding author: Lidia Glodzik, Center for Brain Health, Department of Psychiatry, NYU School of Medicine, 145 East 32nd Street, New York NY, 10016. Tel: (212) 263-5698, Fax: (212) 263-3270; Lidia.Glodzik@nyumc.org.

Conflict of Interest statement

Drs. Mosconi, Tsui and de Leon have a patent on a technology that was licensed to Abiant Imaging Inc. by NYU and, as such, have a financial interest in this license agreement and hold stock and stock options on the company. Drs. Mosconi and de Leon have received compensation for consulting services from Abiant Imaging.

Other authors have nothing to disclose.

Pittsburgh compound B (PiB) is the first and most widely used positron emission tomography (PET) tracer to detect cortical amyloid plaques, a pathological hallmark of Alzheimer's disease (AD) [1]. An interesting feature of PiB is its significant retention in the cerebral white matter (WM). While the reason for PiB binding in the WM remains unclear, data link it to the lipophilic character of PiB [1] and high WM lipid content. Moreover, both healthy subjects and AD patients have low PiB delivery to WM and slow WM PiB clearance [1]. Although direct comparisons between AD and NL groups show no differences in WM PiB clearance [2] or WM PiB signal intensity [1, 3], in healthy controls with no cortical retention, slower PiB clearance from WM than from gray matter (GM) results in distinct images where WM intensity exceeds cortical signal. This effect is especially evident at later acquisition times. This characteristic picture gave rise to the possibility that PiB can be used as a WM tracer [4, 5]. Indeed, some researchers used PiB to image multiple sclerosis (MS) patients and noted a significant reduction in PiB uptake in demyelinated plaques in comparison with normal appearing white matter (NAWM) [4].

White matter lesions (WML) are common among the elderly and constitute a wide range of histopathological changes [6]. While they alter tissue properties, their interactions with PiB have not yet been studied. Because WM hyperintensities are prevalent in the older population, which is currently the main target of amyloid imaging, it is vital to understand how WML affect amyloid scans. To answer this question, we examined PiB retention in WML and the NAWM.

METHODS

Subjects

The study included seventy-three subjects (mean age 61.9±10.0 years, 71% women, education 17±2.0 years). All participants signed IRB-approved consents for protocols investigating risk factors of cognitive decline and Alzheimer's disease. All individuals underwent extensive medical, psychiatric, and neurological examinations and had a lab work-up. All were diagnosed as cognitively healthy, with Mini Mental State Examination ≥26 points and Clinical Dementia Rating=0. The study excluded subjects scoring >16 on the 17-item Hamilton Depression Scale [7], as well as subjects with brain tumors, neocortical infarction, diabetes, substance abuse, and psychotic disorders.

Imaging

MRI acquisition—Imaging was performed on a 1.5T GE scanner (GE, Milwaukee, WI, USA). The protocol consisted of T1 weighted 3D Fast Gradient Echo (coronal orientation, repetition time [TR]=35ms, time to echo [TE]=2ms, flip angle [FA]=60°, number of excitations [NEX]=1, slice thickness: 1.6mmGE) and 2D fluid attenuation inversion recovery (FLAIR) (axial orientation, TR 9279ms, TE 127ms, TI 2300ms, FA 90°, NEX=1, 32 slices 3.3mm thick).

Whole brain volumes—Brain parenchyma volume, V_B, was obtained by automatic segmentation of T1 weighted images [8]. The process began by finding a "pure WM" seed, defined as a 1-cm cubic region with a minimal coefficient of variability of T1 signal. An

initial mask M_0 was then constructed from voxels with signal >0.55 relative to the seed signal. Next, cerebrospinal fluid (CSF) spaces were excluded, and the head/neck muscles and optic nerves were disconnected using subvoxel erosion with a 2.7mm radius. The program then computed the largest connected components of the eroded mask. A constrained growth operator was applied to generate the brain parenchyma mask M. The brain stem, the pons and the cerebellum were retained in M. V_B is the product of the number of voxels in M by the voxel volume [8].

WML segmentation—FLAIR images were first corrected for signal non-uniformity with the N3 algorithm. We then created the brain mask M (see above). In order to assure that hyperintensities located at the ventricular border were considered, we created a set M′ by applying the 3D morphologic fill operator to M. Next we created the set L_0, containing voxels in M′ with signal 2.5 standard deviations above the mean FLAIR signal for M. L_0 was filtered to a) remove cortical voxels located within 3 mm of the surface of M, b) small clusters of volume <12mm^3 (presumed to represent image noise), and c) connected regions having >50% CSF border (presumed to represent the choroid plexus and the septum). WML volume V_{WML} was the product of the FLAIR voxel volume and the number of voxels within the WML mask. The fractional WML volume fV_{WML} was generated as V_{WML}/V_B.

We have previously analyzed the accuracy of this method [9] by comparing it against hand-segmentation of WML. The reference (manual tracing) distribution of lesion volumes V was 4.6 ± 7.6 cm^3. V measured by the automatic tool at 2.5 standard deviations (SD) was 5.9 ± 7.1 cm^3. There was a highly significant linear relationship (adjusted R^2=0.972, df=72, p<0.0001) between automatic and manual V. The automatic segmentation was characterized by a significant multiplicative oversegmentation bias, averaging 1.36 cm^3. When automatically computed lesion volumes were calibrated to remove that bias, the mean absolute error was reduced to 0.94 cm^3. When we used 2 SD to define WML, the bias was significantly larger than for 2.5 SD. When we used 3 SD, the correlation with reference measures was reduced.

WML volume was subdivided into periventricular (PWML) and deep (DWML). First, we generated the ventricular mask (M′-M) by calculating the set difference between the filled brain mask M′ and the brain parenchyma mask M. The periventricular region was created by a morphological growth of the ventricular mask by 13mm [10]. PWML were generated by intersecting WML mask with the periventricular region; DWML as the set difference WML – PWML.

V_B and WML volumes were determined using locally developed software *FireVoxel* (https://files.nyu.edu/hr18/public).

PiB-PET acquisition—Scans were performed on an LS Discovery scanner (GE, Milwaukee, WI, USA); 5.4mm full width at half maximum (FWHM), 30 cm field of view. Before scanning, a venous line was inserted in the antecubital vein, and 15 mCi (~550 MBq) of PiB (radiochemical purity >98%) was administered. Scanning started about 60 minutes after injection and lasted 30 minutes. Prior to PET examination, a CT transmission scan was

acquired for attenuation correction. All images were corrected for photon attenuation, scatter, and radioactive decay, and reconstructed into a 512×512 matrix.

PiB-PET and FLAIR image processing—The 60–90 min PiB data was used to generate summed PET images. PiB and FLAIR images (together with corresponding WML masks) were coregistered and resliced to T1 scans using the normalized mutual information algorithm in SPM8. T1-MRI images were previously segmented into gray, white and CSF masks. After coregistration of FLAIR images, a NAWM mask was created as all voxels with probability greater than 99% from T1 segmented WM mask minus WML mask. All cases were successfully inter-modality coregistered and segmented. PiB-FLAIR within subject coregistrations were examined by an experienced observer as (a) variable opacity overlays, (b) overlay of FLAIR brain edges over PiB; all demonstrating good accuracy. Figure 1A shows PiB-FLAIR coregistration for a case with an extreme WML load. Figure 1B represents a case with mild WML, mostly in the frontal region. Figure 2 shows separation of DWML from the total WML mask for cases presented in Figure 1A–B. PiB uptake values were extracted from WML and NAWM masks.

Partial volume correction (PVC) of PiB images was performed using Muller-Gartner's 3-compartment method [11]. First the MRI image segmented into gray matter, white matter, and CSF was modified by convolving it with point-spread function of PET scanner. We have additionally adjusted segmented white and gray matter for lesions before convolution. GE PET scanner with 6mm resolution was assumed. Then the PET images were divided by modified MRI image to provide an estimate of radioactivity concentration.

For PiB images, a cerebellar region of interest (ROI), sampling posterior lobe cortex between the primary fissure and posterior fissure, was used to extract the cerebellar intensity. This value was used to normalize intensity within NAWM and WML masks.

Statistics

Paired t-test was used to compare PiB retention in NAWM and WML.

RESULTS

The mean fV_{WML} was .45±.80%; for PWML it was .35±.58%, for DWML .11±.24%.

PiB binding within WML was reduced by 14.6% compared to NAWM, (t_{72}=15.8, p<.001). This was true both for PWML (t_{72}=17.8, p<.001, 17.4% reduction) and DWML (t_{72}=4.5, p<.001, 7.5% reduction). The signal in PWML was also significantly lower than in DWML (t_{72}=5.6, p<.001, 11% reduction) (Table 1).

DISCUSSION

PiB signal is significantly lower within FLAIR hyperintensive lesions than in the NAWM. Since PiB-PET images have lower resolution than FLAIR, with a blurry ventricular border, we performed partial volume correction and examined PWML and DWML separately, to test the possibility that our findings were confounded by partial volume effects. The reduction was significant in our PVC data both in PWML and DWML, although the effect

in PWML was stronger than in DWML. We conclude that our results are not biased by partial volume artifacts.

There has been a growing interest in the relationship between PiB deposition and WML. However, most of the papers examined the association between WML and PiB uptake in cerebral GM, i.e. investigating the influence of WML on progression of cortical PiB accumulation [12], how WML and GM PiB interact to predict AD diagnosis [13], or whether WML facilitates cortical amyloid deposition [14]. None of them addressed PiB retention in WM.

The target of PiB binding in the WM is poorly understood. It was shown that this binding is non-specific since it is non-displaceable [1] and non-saturable [2]. The lipophilic character of PiB [1] and the high lipid content of WM may explain our observation. Since WML constitute areas of demyelination, and consequently loss of lipids, WML could manifest as a lower PiB signal. Second, myelin basic protein (MBP) is one of the major protein components of myelin [15]. In the presence of lipids, MBP takes a form of a β-sheet [15], which is a target for PiB binding. MBP is reduced in WML [16], and as a result, WML would retain less PiB, consistent with our finding.

Using autofluorescence measurements, Stankoff at el. found that PiB stained WM tracts in brain sections from mice and humans. Moreover, in the brains of MS patients, the same staining clearly identified fully and partially demyelinated lesions [4], possibly reflecting the amount of MBP. However, Fodero-Tavoletti et al. did not observe staining of WM tracts with PiB in AD or control brain sections [2]. Also, autoradiographic experiments did not show [^{3}H]PiB binding to WM tracts in patients with traumatic brain injury (TBI) [17].

The average decrease in WML PiB signal in our subjects was 14%, less than the ~30% reported previously for those with demyelinating MS lesions [4]. This supports the finding that WML demyelination is less pronounced and coexists with other pathologies in aging, while it is a dominant feature in MS. Also in line with our findings, Hong et al. observed that although TBI patients showed somewhat greater PiB binding in WM structures than controls, regions with a high signal on FLAIR images showed no increase in PiB retention [17].

In a recent PET study of a rat demyelination model, a strong correlation was found between de/remyelination scores and PiB binding within the lesions [5]. Moreover, PiB was the only one out of three tracers to correctly detect remyelination. In our study, reduction in PiB retention was greater in PWML than in DWML. Although both PWML and DWML present with myelin loss and pallor [6], some found that PWML displayed greater MBP loss on immunohistochemical staining than DWML [16]. Furthermore, in our group the mean PWML volume was higher than DWML. This indicates that, as previously reported [16], PWML appear earlier, progress faster and exhibit greater MBP loss.

There are several clinical implications of our findings:

- In healthy younger controls without WML, one should expect high PiB contrast between WM and GM.

- In an older population, where both WML and amyloid are prevalent, the attenuation of PiB WM signal related to WML may improve conspicuity of GM tracer uptake.
- This phenomenon could be even more pronounced in AD patients who often present with a high WML load.
- In cases with low cortical amyloid deposition combined with neighboring WML and extensive atrophy, the cortical PiB signal could be diluted by a lower WM signal, causing a false negative interpretation.

The limitations of our paper include lack of kinetic data. We were only able to present retention 60–90 min post-injection. Another limitation is the lack of pathologic post-mortem confirmation of our results. Future studies with pharmacological blocking of PiB are warranted.

In conclusion, PiB binding in WM is influenced by the presence of WML, which lower the signal. Although this phenomenon may complicate image interpretation only in a limited group of subjects, it adds to the growing evidence that PiB is a sensitive marker of WM injury and prompts further investigations into PiB binding targets in WM.

Acknowledgments

We gratefully acknowledge support from NIA grants 2R01AG013616-22, R01-AG035137, RC2-AG036502, P30 AG008051 and HL111724-01.

Reference List

1. Klunk WE, Engler H, Nordberg A, Yanming W, Blomqvist G, Holt DP, et al. Imaging brain amyloid in Alzheimer's disease with Pittsburgh Compound-B. Ann Neurol. 2004; 55(3):306–319. [PubMed: 14991808]
2. Fodero-Tavoletti MT, Rowe CC, McLean CA, Leone L, Li Q-X, Masters CL, et al. Characterization of PiB binding to white matter in Alzheimer disease and other dementias. The Journal of Nuclear Medicine. 2009; 50:198–204.
3. Rowe CC, Ng S, Ackermann U, Gong SJ, Pike K, Savage G, et al. Imaging β-amyloid burden in aging and dementia. Neurology. 2007; 68(20):1718–1725. [PubMed: 17502554]
4. Stankoff B, Freeman L, Aigrot MS, Chardain A, Dolle F, Williams A, et al. Imaging central nervous system myelin by positron emission tomography in multiple sclerosis using [methyl-11C]-2-(4′-methylaminophenyl)- 6-hydroxybenzothiazole. Ann Neurol. 2011; 69(4):673–680. [PubMed: 21337603]
5. de Paula Faria D, Copray S, Sijbesma JWA, Willemsen ATM, Buchpiguel CA, Dierckx RAJO, et al. PET imaging of focal demyelination and remyelination in a rat model of multiple sclerosis: comparison of [11C]MeDAS, [11C]CIC and [11C]PIB. European Journal Of Nuclear Medicine And Molecular Imaging. 2014; 41:995–1003. [PubMed: 24499866]
6. Gouw AA, Seewann A, van der Flier WM, Barkhof F, Rozemuller AM, Scheltens P, et al. Heterogeneity of small vessel disease: a systematic review of MRI and histopathology correlations. Journal of Neurology, Neurosurgery & Psychiatry. 2011; 82:126–135.
7. Bech P, Kastrup M, Rafaelsen OJ. Mini-compendium of rating scales for states of anxiety depression mania schizophrenia with corresponding DSM-III syndromes. Acta Psychiatr Scand Suppl. 1986; 326:1–37. [PubMed: 3458353]
8. Mikheev A, Nevsky G, Yitta S, Grosmann R, Rusinek H. Fully automated segmentation of the brain from T1-weighted MRI using Bridge Burner algorithm. Journal of Magnetic Resonance Imaging. 2008; 27(6):1235–1241. [PubMed: 18504741]

9. Rusinek H, Glodzik L, Mikheev A, Zanotti A, Li Y, de Leon M. Fully automatic segmentation of white matter lesions: error analysis and validation of a new tool. Intern J Computer Assisted Radiology & Surgery. 2013; 8 (suppl 1):289–291.

10. Sachdev P, Chen X, Wen W. White matter hyperintensities in mid-adult life. Curr Opin Psychiatry. 2008; 21:268–274. [PubMed: 18382226]

11. Muller-Gartner HW, Links JM, Prince JL, Bryan RN, McVeigh E, Leal JP, et al. Measurement of radiotracer concentration in brain gray matter using positron emission tomography: MRI-based correction for partial volume effects. J Cereb Blood Flow Metab. 1992; 12:571–583. [PubMed: 1618936]

12. Grimmer T, Faust M, Auer F, Alexopoulos P, Forstl H, Henriksen G, et al. White matter hyperintensities predict amyloid increase in Alzheimer's disease. Neurobiol of Aging. 2012; 33:2766–2773.

13. Provenzano FA, Muraskin J, Tosto G, Narkhede A, Wasserman BT, Griffith EY, et al. White matter hyperintensities and cerebral amyloidosis. JAMA Neurology. 2013 Published online February 18, 2013. 10.1001/jamaneurol.2013.1321

14. Noh Y, Seo SW, Jeon S, Lee JM, Kim JH, Kim GH, et al. White matter hyperintensities are associated with amyloid burden in APOE4 non-carriers. Journal of Alzheimer's Disease. 2014; 40(4):877–886.

15. Harauz G, Ishiyama N, Hill CMD, Bates IR, Libich DS, Fares C. Myelin basic protein -diverse conformational states of an intrinsically unstructured protein and its roles in myelin assembly and multiple sclerosis. Micron. 2004; 35(7):503–542. [PubMed: 15219899]

16. Murray ME, Vemuri P, Preboske GM, Murphy MC, Schweitzer KJ, Parisi JE, et al. A quantitative postmortem MRI design sensitive to white matter hyperintensity differences and their relationship with underlying pathology. Journal of Neuropathology & Experimental Neurology. 2012; 71(12)

17. Hong YT, Veenith T, Dewar D, Outtrim JG, Mani V, Williams C, et al. Amyloid imaging with carbon 11C-labeled Pittsburgh compound B for traumatic brain injury. JAMA Neurology. 2014; 71(1):23–31. [PubMed: 24217171]

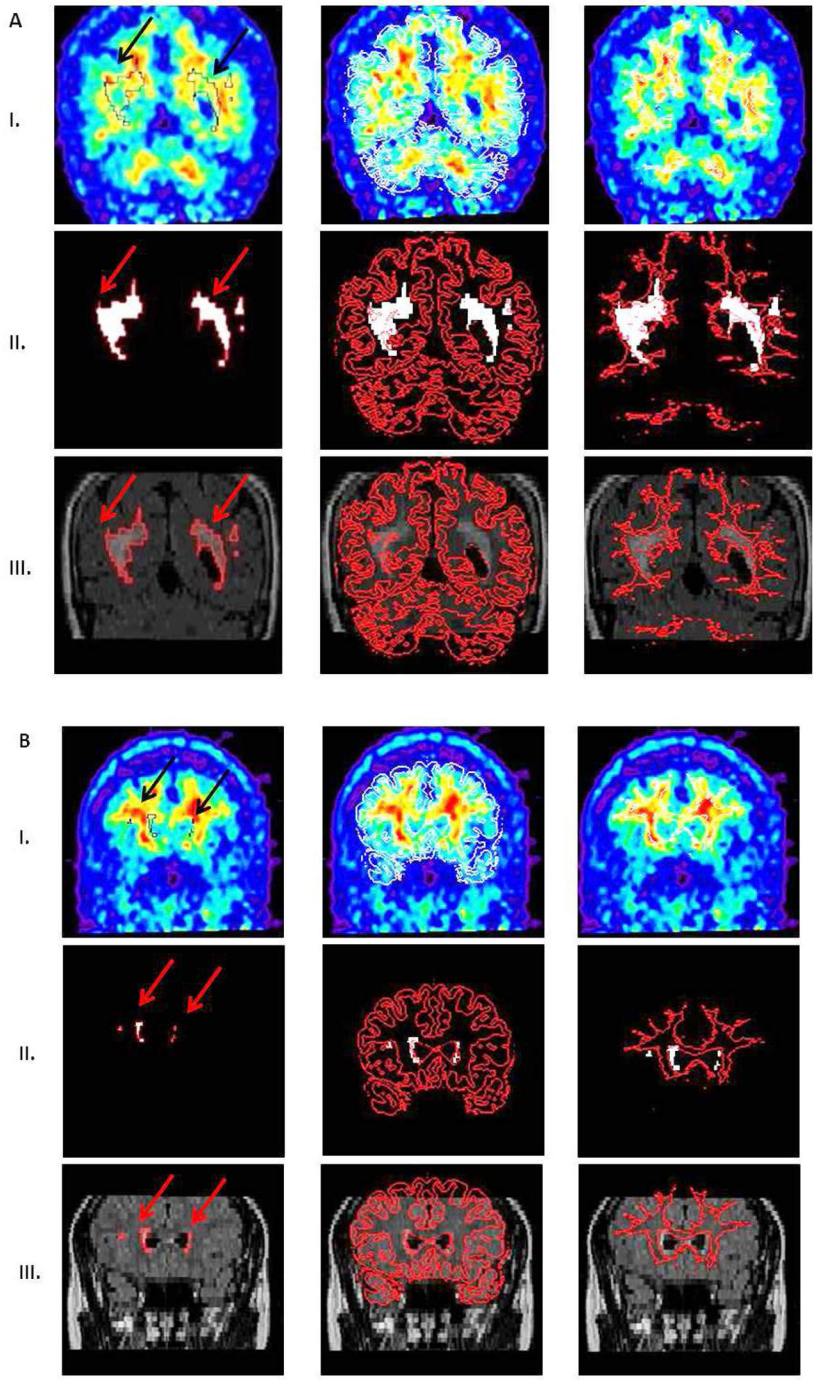

Figure 1.

A. Coregistration of FLAIR and PiB images for a case with extremely high white matter lesions (WML) load. Row I represents PiB images with superimposed masks: WML (first column, black outline indicated by black arrows), gray matter (GM) obtained from T1 segmentation (second column white outline), and normal appearing white matter (NAWM) (third column, white outline).

Row II represents WML mask (white outlined in red, red arrows). Superimposed GM and NAWM masks are outlined in red.
Row III: FLAIR images with superimposed WML (red arrows), GM, and NAWM masks, respectively.
B. Coregistration of FLAIR and PiB images for a case with very mild WML load, mostly in the frontal region. Images in rows I–III as in Figure 1A.

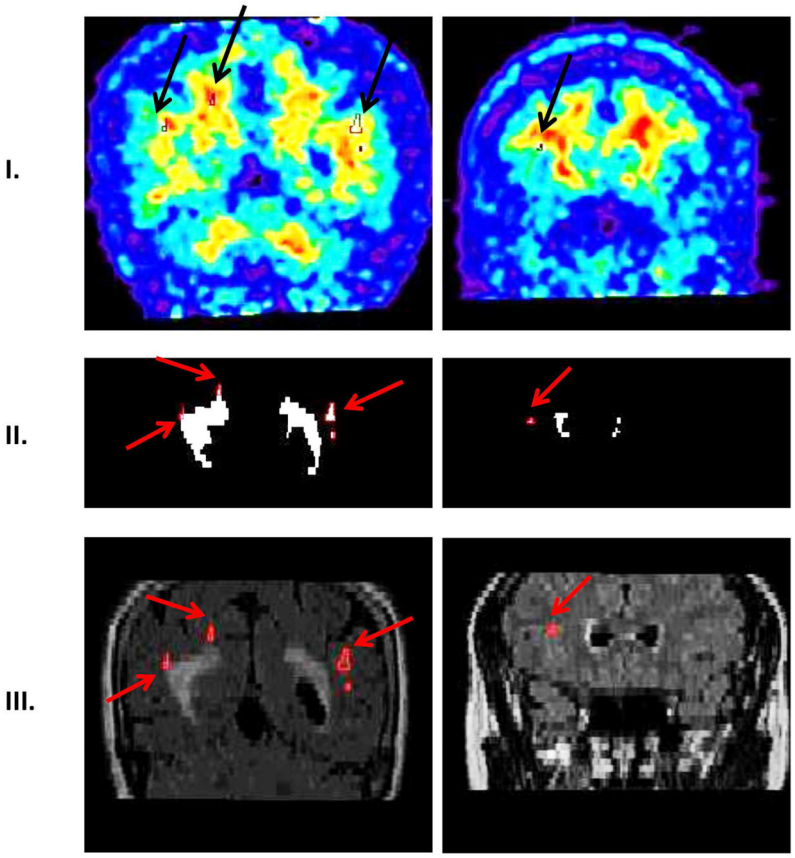

Figure 2.

Separation of deep WML (DWML) from the WML mask. Row I shows PiB images (DWML outlined in black with black arrows). Row II shows WML mask (DWML outlined in red with red arrows). Row III shows FLAIR images (DWML outlined in red with red arrows). First column represents case presented in Figure 1A, second column case presented in Figure 1B.

Table 1

PiB uptake within WM regions presented as standardized uptake value ratios to cerebellum.

Region	ROI to cerebellum ratio
Normal-appearing white matter	1.72 ± .23
White matter lesions	1.47 ± .24*
Periventricular WML	1.42 ± .24*
Deep WML	1.59 ± .33*

* significantly different from NAWM at p<.001